Isomorphously Substituted [Fe,Al]ZSM-5 Catalysts for Methane Dehydroaromatization

ACS Catalysis

pubs.acs.org/acscatalysis

Research Article

Isomorphously Substituted [Fe,Al]ZSM-5 Catalysts for Methane Dehydroaromatization

Yujie Liu, Aleksei Bolshakov, Marita Ćoza, Victor Drozhzhin, Emiel J. M. Hensen, and Nikolay Kosinov*

Cite This: *ACS Catal.* 2023, 13, 8128–8138

Read Online

ACCESS | Metrics & More | Article Recommendations | Supporting Information

ABSTRACT: Dehydroaromatization of methane (MDA) under non-oxidative conditions is a promising reaction for direct valorization of natural gas and biogas. Typically, Fe-modified ZSM-5 catalysts display low aromatic productivity and high coke selectivity in the MDA reaction. Herein, we show the benefit of starting from isomorphously substituted Fe-sites in [Fe,Al]ZSM-5 zeolites prepared by direct hydrothermal synthesis. Upon calcination, these samples contain predominantly isolated Fe^{3+} species, either atomically dispersed within the zeolite framework or anchored at exchange sites inside zeolite channels. In terms of the integral hydrocarbon productivity, [Fe,Al]ZSM-5 catalysts outperform Fe/ZSM-5, prepared by impregnation, as well as Mo/ZSM-5 catalysts with the same Si/Al ratio and molar metal loading. Operando X-ray absorption spectroscopy coupled with mass spectrometry (XANES-MS) demonstrates that the initial tetrahedral Fe^{3+} within the zeolite framework or at exchange sites are transformed into octahedral extraframework Fe^{2+} active sites during the MDA reaction and form small Fe_2O_3 clusters during oxidative regeneration. Combining activity measurements and operando thermogravimetry shows that the duration of the induction period, related to the formation of active hydrocarbon pool intermediates, strongly depends on the Fe dispersion and loading and can be used as a suitable descriptor for the MDA activity of [Fe,Al]ZSM-5. The shorter induction period of [Fe,Al]ZSM-5 in comparison to impregnated Fe/ZSM-5 can be linked to the higher methane conversion rate over highly dispersed Fe-sites and faster formation of active hydrocarbon pool intermediates.

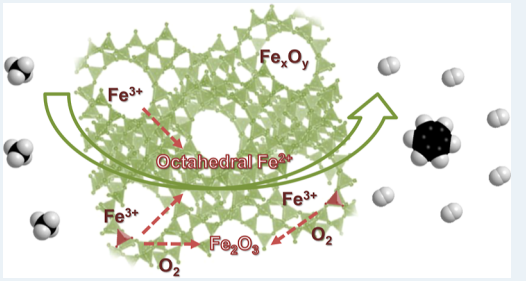

KEYWORDS: *methane dehydroaromatization, ZSM-5, Fe, isomorphous substitution, hydrocarbon pool*

1. INTRODUCTION

Direct conversion of abundant methane to valuable liquid hydrocarbons has drawn the attention of the catalysis community.[1] Methane dehydroaromatization (MDA) under non-oxidative conditions is an attractive route for the direct conversion of methane to value-added aromatics (mainly benzene and naphthalene) and CO_x-free hydrogen. Thermodynamically limited methane conversion of up to 12% with benzene selectivity up to 80% can be achieved over widely studied Mo/ZSM-5 catalysts at 700 °C and atmosphere pressure.[2,3] Unfortunately, the commercial application of conventional Mo/ZSM-5 catalysts for the MDA reaction is hampered by their rapid coking deactivation and insufficient activity.[4]

Fe-containing ZSM-5 zeolites are interesting alternatives to Mo/ZSM-5 for industrial applications, owing to the high abundance and low price of the base metal Fe. While Fe/ZSM-5 typically deactivates slower than Mo/ZSM-5 and it has a higher stability under oxidative regeneration conditions, its catalytic activity and benzene selectivity are significantly lower.[5,6] To enhance the MDA activity of Fe/ZSM-5 catalysts, it is necessary to understand the nature of Fe-species in the working catalysts and maximize the concentration of the most active sites. Considerable efforts have been made to identify the structure of Fe-sites during the MDA reaction. It is still under debate whether Fe oxides/carbides/single atoms or Fe-cations stabilized on zeolite Brønsted acids sites are the active phases for methane activation. For example, Weckhuysen et al. proposed that Fe_3O_4 derived from partial reduction of Fe_2O_3 is the active phase for the MDA reaction in Fe/ZSM-5 catalysts.[7] Using X-ray photoelectron spectroscopy and X-ray diffraction (XRD), Tan found that Fe_2O_3, located on the external surface of HZSM-5 and HMCM-22 zeolites with 6 wt % Fe, was gradually reduced to metallic Fe and then carburized to Fe-carbide.[8] The author proposed that both metallic Fe and Fe-carbide were effective for methane activation, while only the latter was responsible for the aromatization of methane. Guo et al. synthesized a zeolite-free $FeSiO_2$ catalyst with single Fe atoms embedded into a SiO_2 matrix. High methane conversion (~40%) and hydrocarbon (ethylene, benzene, and naphthalene) selectivity (> 99%) at a high reaction temperature of

Received: February 23, 2023
Revised: May 12, 2023
Published: June 2, 2023

https://doi.org/10.1021/acscatal.3c00854
ACS Catal. 2023, 13, 8128–8138

1090 °C were achieved.[9] More recently, using a combination of the pulse reaction technique, X-ray adsorption spectroscopy (XAS) and DFT analysis, Vollmer et al. concluded that iron oxycarbide FeO_xC_y clusters form the active phase in MDA catalysts.[10]

Instead of the traditional impregnation method, Xu et al. used a liquid ion-exchange catalyst synthesis method and showed that Fe^{2+}-exchanged Fe/ZSM-5 catalysts are more active and selective for the production of aromatics than Fe^{3+}-exchanged counterparts.[11] Using isomorphous substitution, wet ion exchange, and core−shell synthetic approaches, Lai and Veser found that the formation of aromatics can be attributed to the concentration of highly dispersed Fe-sites located in the zeolite channels.[12] These results together with several other reports indicate that isolated Fe-species are the preferred precursors to highly active sites for the MDA reaction, while larger Fe clusters present on the zeolite external surface are spectators and mainly contribute to coke formation.[11−14] Fe/ZSM-5 catalysts prepared by impregnation usually contain a wide range of Fe-species, different in size and chemical nature (isolated Fe, oligomeric Fe clusters, and Fe_2O_3 nanoparticles). Diversity of these Fe-precursors results in the formation of a mixture of Fe-species with different reduction/carburization degree during the MDA reaction. This hampers the elucidation of active sites and the establishment of structure-activity relationships. To resolve the nature of the active Fe-sites and enhance the MDA activity of Fe-based catalysts, it would be advantageous to prepare highly dispersed Fe/ZSM-5 catalysts with a homogeneous distribution of Fe-species.

In this work, we studied the evolution and structure of active Fe-species under harsh conditions of the MDA reaction and oxidative regeneration. First, a series of isomorphously substituted [Fe,Al]ZSM-5 catalysts with highly dispersed Fe-species were obtained by one-step hydrothermal synthesis and applied for the MDA reaction. Second, using a combination of XRD, Ultraviolet−visible (UV−vis) spectroscopy, temperature-programmed reduction in hydrogen (H_2-TPR), and Fourier transformation infrared spectroscopy of adsorbed pyridine (Py-FTIR), we determined the distribution of Fe-sites in [Fe,Al]ZSM-5 catalysts. Furthermore, we tracked the evolution of active Fe-sites during the MDA reaction and isothermal oxidative regeneration with operando X-ray absorption near edge structure coupled with mass spectrometry (XANES-MS) and extended X-ray absorption fine structure (EXAFS). Finally, combining operando thermogravimetric analysis and mass spectrometry (TGA-MS) with ex situ TGA, we studied the growth and properties of formed carbon deposits, and correlated them with the catalytic activity of [Fe,Al]ZSM-5 catalysts. The identification of active Fe-sites and improved MDA activity of [Fe,Al]ZSM-5 catalysts emphasize the importance of Fe dispersion and provide opportunities for designing better Fe-based catalysts for the MDA reaction.

2. EXPERIMENTAL SECTION

2.1. Catalyst Preparation. *2.1.1. Isomorphously Substituted [Fe,Al]ZSM-5.* [Fe,Al]ZSM-5 zeolites were synthesized using tetrapropylammonium hydroxide (TPAOH, Merck, 40 wt %) as the template. To prepare the samples with high Fe loading (≥1.6 wt %), we, first, dissolved $Al(OH)_3$ (Sigma-Aldrich, reagent grade) in a mixture of deionized water and TPAOH in a PP bottle.

The zeolite samples with low Fe concentration were synthesized without the addition of NaOH (Si/OH = 250/45). After tetraethyl orthosilicate (TEOS, Merck, 99%) was added dropwise, the solution was stirred for 5 h at room temperature. The molar composition of the synthesis gel was

$$45\ \mathrm{TPAOH}:\ y\ \mathrm{Fe_2O_3}:\ 3.125\ \mathrm{Al_2O_3}:\ 250\ \mathrm{SiO_2}:\ 3750\ \mathrm{H_2O} (y = 1.5 \text{ or } 1.865)$$

We note that Fe^{3+} can be incorporated into the zeolite framework, rendering the zeolite framework negatively charged in the same manner as Al^{3+} incorporation does. To increase the Fe content of the ZSM-5 zeolite framework, a higher concentration of charge-compensating cations (e.g., Na^+) is needed. Thus, the zeolite samples with high Fe concentration were synthesized with addition of NaOH and kept pH the same (Si/OH = 250/45).

After the addition of TEOS, the solution was stirred for 2 h at room temperature. Then, NaOH (50 wt % in water, Sigma-Aldrich) was added into the formed gel. After stirring for 3 h, aqueous solution of $Fe(NO_3)_3{\cdot}9H_2O$ (Thermo Fisher Scientific) of appropriate concentration was added and further stirred for 0.5 h, until a dense gel was formed. The final gel composition was as follows

$$35\ \mathrm{TPAOH}:\ x\ \mathrm{Fe_2O_3}:\ 5\ \mathrm{Na_2O}:\ 3.125\ \mathrm{Al_2O_3}:\ 250\ \mathrm{SiO_2}:\ 3750\ \mathrm{H_2O} (x = 2.5,\ 3.125 \text{ or } 3.57)$$

Crystallization was carried out in a Teflon-lined autoclave under tumbling (50 rpm) at 175 °C for 9 days. After crystallization, the solids were filtered, washed, and dried at 110 °C overnight, followed by a calcination step at 550 °C for 4 h to remove the occluded organic template inside the pores. Finally, the zeolite materials were ion-exchanged three times with 1 mol/L NH_4NO_3 solution at 70 °C for 3 h (1 g of the solid per 100 mL), followed by drying and calcination at 550 °C for 7 h to obtain their H-forms. The resulting materials were pelletized and sieved to 250−500 μm, and denoted as *x* % [Fe,Al]ZSM-5, where *x* indicates the actual Fe loading in wt %.

2.1.2. Fe-Free ZSM-5, Impregnated Fe/ZSM-5 and Mo/ZSM-5. Fe-free ZSM-5 zeolite was also synthesized by following a similar procedure, with the synthesis gel composition of 45 TPAOH:3.125 Al_2O_3:250 SiO_2:3750 H_2O or 35 TPAOH:5 Na_2O:3.125 Al_2O_3:250 SiO_2:3750 H_2O. The zeolite material obtained without and with NaOH addition were denoted as [Al]ZSM-5_N and [Al]ZSM-5. Afterward, impregnated samples 1.0% Fe/ZSM-5 (0.17 mmol/g Fe) and 1.6% Fe/ZSM-5 (0.28 mmol/g Fe) were prepared by incipient wetness impregnation using [Al]ZSM-5 zeolite in the H-form. The same approach was employed to prepare 1.8% Mo/ZSM-5 (0.19 mmol/g Mo) and 2.8% Mo/ZSM-5 (0.29 mmol/g Mo) catalysts.

Impregnation was performed with aqueous solution of $Fe(NO_3)_3{\cdot}9H_2O$ (Thermo Fisher Scientific) or $(NH_4)_6Mo_7O_{24}{\cdot}4H_2O$ (Merck). The as-prepared samples were dried and calcined at 550 °C for 8 h. After pelletizing and sieving to 250−500 μm, the resulting materials were named as *y* % Fe/ZSM-5 or *z* % Mo/ZSM-5, where *y* and *z* represent the Fe and Mo loading on impregnated Fe and Mo samples, respectively.

https://doi.org/10.1021/acscatal.3c00854
ACS Catal. 2023, 13, 8128−8138

2.2. Catalyst Characterization. The Si/Al ratio and Fe loading of zeolites were determined by inductively coupled plasma optical emission spectroscopy (ICP-OES, Spectro CIROS CCD). Prior to the measurements, samples were dissolved in a mixture of HF (40%), HNO_3 (60%), and H_2O, with a ratio of 1:1:1 by weight.

Surface areas and pore volumes of zeolites were analyzed by argon physisorption at −186 °C, with a Micromeritics ASAP 2020 instrument. The samples were degassed at 300 °C for 8 h under vacuum before the measurements. The specific areas of zeolites were calculated using the Brunauer−Emmett−Teller method. *t*-plot method was applied for the evaluation of micropore surface areas and volumes of zeolites.

XRD patterns of fresh and spent samples were performed on a Bruker D2 powder diffractometer using Cu Kα radiation. The 2θ range of 5−50° and scan speed at 0.01°/s were used. The relative crystallinity of zeolites (with [Al]ZSM-5 of 100%) was calculated by summing the area at 23.1, 23.3, 23.7, 24.0, and 24.4°.

The morphologies of zeolites were characterized by scanning electron microscopy (SEM). Images were recorded on a FEI Quanta 200F SEM at 3 kV, with a spot size of 4.5. Transmission electron microscopy (TEM) images of samples were obtained using a FEI Tecnai 20 instrument at 200 kV.

Diffuse reflectance UV−vis spectra were recorded on a Shimadzu spectrometer (UV-2401PC), with $BaSO_4$ as a reference. The recorded wavelength is in the range of 200−800 nm.

Temperature-programmed reduction in hydrogen (H_2-TPR) was performed using a Micromeritics Autochem II 2920 instrument. About 50 mg of fresh catalyst was loaded in a U-shaped quartz reactor and heated up to 900 °C at a rate of 5 °C/min, in a H_2/N_2 mixture flow (50 mL/min, 4 vol % of H_2).

Fourier-transform infrared spectroscopy of adsorbed pyridine (Py-FTIR) spectra were recorded on a Bruker Vertex 70v FTIR spectrometer. Prior to the measurements, the sample wafer (about 15 mg, diameter of 1.3 cm) was pre-treated in air flow at 550 °C for 1 h. Afterward, it was cooled down to 150 °C for background spectrum recording and pyridine adsorption. The desorption of pyridine in vacuum was carried out at 150, 250, 350, and 450 °C. The corresponding IR spectra were recorded at 150 °C, at a 2 cm^{-1} resolution and averaging of 32 scans. The spectra were normalized by the sample weight after background subtraction.

The coke content accumulated on spent catalysts was determined by ex situ TGA, using a Mettler Toledo TGA/DSC 1 instrument. Approximately 25 mg of a spent sample was loaded in an uncovered alumina crucible. Upon increasing the temperature from 40 to 800 °C, at a rate of 5 °C/min in O_2/He mixed flow (60 mL/min, O_2/He = 1:2).

Operando TGA-MS coupled measurements were carried out in a mixed CH_4/Ar flow (22 mL/min, CH_4/Ar = 10:1). A thermogravimetric analyzer (TG, Discovery HP TGA 75, TA Instruments) was used for tracking the weight changes and a mass spectrometer (MS, GeneSys, ESS) for monitoring the evolved gases obtained during the MDA reaction, like H_2 (m/z = 2), CH_4 (m/z = 16), CO or C_2H_4 (m/z = 28), CO_2 (m/z = 44), and C_6H_6 (m/z = 78). For each test, about 10 mg of fresh catalyst was loaded in an uncovered alumina crucible. The system was first heated to 400 °C at a rate of 10 °C/min, and then kept at 400 °C for 30 min. Afterward, the temperature was increased to 700 °C, at the ramping rate of 10 °C/min. The same treatment was applied to the empty crucible to obtain a background signal.

The oxidation state and geometry of Fe-species in catalysts were studied by XAS at Balder beamline (MAX IV Laboratory in Lund, Sweden). X-ray absorption near edge structure (XANES) spectra were recorded at Fe K-edge (7112 eV) in the transmission mode. The X-ray energy was selected using a Si(111) crystal monochromator. Fe foil was employed for the calibration of energy. Athena software (Demeter v.0.9.26) was used for the normalization of XANES spectra and Artemis software for the analysis of EXAFS spectra.[15]

2.3. Catalyst Tests. *2.3.1. MDA Reaction.* The MDA reaction was conducted in a home-made quartz reactor (i.d. 4.0 mm, o.d. 8.0 mm, length 450 mm) with online gas chromatograph (Compact GC 4.0, Global Analyzer Solutions) for product analysis. For tests, 300 mg of sieved catalyst (250−500 μm) was placed between two quartz wool plugs and mounted in the isothermal (700 °C) zone in the reactor. For each test, a mixed CH_4/Ar flow with Ar as an internal standard (30 mL/min, CH_4/Ar = 95:5) was used. The reactor was first heated up to 450 °C and kept at 450 °C for 45 min. Then, the temperature was increased to 700 °C at the ramping rate of 15 °C/min. The reactor effluent mixture was separated and analyzed continuously by an online GC, which has been described in detail before.[16]

The presented catalytic results are averaged from three identical experiments. Methane conversion (eq 1), total converted methane along the 1000 min of the reaction (eq 2), carbon yields (eq 3), and carbon selectivity of a certain product (eq 4) were determined, based on the carbon balance

$$\text{conversion}\ (\%) = \frac{N_{\text{carbon}}^{\text{inlet CH}_4} - N_{\text{carbon}}^{\text{outlet CH}_4}}{N_{\text{carbon}}^{\text{inlet CH}_4}} \times 100 \tag{1}$$

$$\text{total converted CH}_4\ (\text{mmol/g}) = \frac{N_{\text{carbon}}^{\text{inlet CH}_4} \sum_{i=0}^{1000} \text{conversion}}{\text{sample weight}} \tag{2}$$

$$\text{yield}\ (\%) = \frac{N_{\text{carbon}}^{\text{product}}}{N_{\text{carbon}}^{\text{inlet CH}_4}} \times 100 \tag{3}$$

$$\text{selectivity}\ (\%) = \frac{\text{yield}}{\text{conversion}} \times 100 \tag{4}$$

2.3.2. Operando XANES-MS Experiments. Operando XANES-MS experiments were carried out at Balder beamline (MAX IV). For each test, an amount of 10 mg of sieved catalyst (125−250 μm) was loaded in a thin quartz capillary (i.d. 1.5 mm, wall thickness 0.01 mm, and length 80 mm), and a CH_4 flow of 5 mL/min was employed. First, the catalyst was heated to 700 °C at a rate of 10 °C/min and kept at 700 °C for 4−8 h, depending on the catalyst. Oxidative regeneration was carried out with partially deactivated catalysts in an O_2 flow of 5 mL/min and at 550 °C for 0.5−1.5 h. After the regeneration process, the catalyst was cooled down in a He flow of 5 mL/min to room temperature. Then, the second MDA reaction was performed on the regenerated catalyst in a CH_4 flow of 5 mL/min. XANES spectra and MS signals were collected simultaneously.

https://doi.org/10.1021/acscatal.3c00854
ACS Catal. 2023, 13, 8128−8138

3. RESULTS AND DISCUSSION

3.1. Fe Speciation in [Fe,Al]ZSM-5. We employed several characterization techniques to study the distribution of Fe-species in the fresh [Fe,Al]ZSM-5 catalysts, which were prepared by isomorphous substitution and subsequent ion-exchange and calcination. ICP results show that the Fe loading of [Fe,Al]ZSM-5 is in the range of 0.9−2.0 wt % (Table 1).

Table 1. Characterization of [Fe,Al]ZSM-5 and Fe-Free ZSM-5

sample	Fe loading[a] (wt %)	Si/Al ratio[a]	V_{micro}[b] (cm^3/g)	S_{micro}[b] (m^2/g)	relative crystallinity[c] (%)
[Al]ZSM-5_N		59	0.14	315	100
[Al]ZSM-5		61	0.14	369	100
0.9% [Fe,Al]ZSM-5	0.87	60	0.14	329	100
1.0% [Fe,Al]ZSM-5	1.00	64	0.13	298	101
1.6% [Fe,Al]ZSM-5	1.56	58	0.13	306	98
1.9% [Fe,Al]ZSM-5	1.92	56	0.12	287	100
2.0% [Fe,Al]ZSM-5	1.95	59	0.12	289	102

[a]Fe contents and Si/Al atomic ratio measured or estimated by ICP analysis. [b]Micropore surface areas and volumes estimated by the *t*-plot method. [c]Relative crystallinity calculated using the diffraction peak areas in the region of 22.5−25°.

When the Fe content ≥1.6 wt %, a decrease of the Si/Al ratio is observed, which indicates that the zeolite crystallization process is affected by the Fe^{3+} concentration (Table S1). The [Fe,Al]ZSM-5 samples also exhibit a slight decrease in microporous areas and volumes with the increase in Fe content (Table 1). It should be noted that Fe-free ZSM-5 zeolites were synthesized at the same pH, with NaOH ([Al]ZSM-5) and without NaOH ([Al]ZSM-5_N), possessing similar chemical composition and textural properties (Table 1). This observation also demonstrated that an accurate comparison between [Fe,Al]ZSM-5 catalysts with high (with NaOH) and low loading (without NaOH) of Fe can be ensured. In this study, we chose [Al]ZSM-5 for the preparation of Fe/ZSM-5 and Mo/ZSM-5. The impregnated catalysts have the metal loadings close to the target values, as shown in Table S2.

As shown by Figure 1, all synthesized materials display the typical diffraction peaks of the MFI zeolite structure. With the increase in Fe loading, the relative crystallinity of [Fe,Al]ZSM-5 remains high (≥98%). No additional peaks corresponding to Fe oxides can be found, even at a high Fe loading of 2.0 wt %

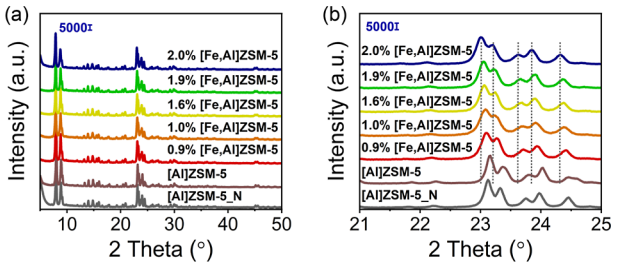

Figure 1. XRD patterns of [Fe,Al]ZSM-5 and Fe-free ZSM-5 in the 2θ range of (a) 5−50 and (b) 21−25°.

(Figures 1 and S1). It should be noted that, compared to [Al]ZSM-5, the diffraction peaks of [Fe,Al]ZSM-5 are slightly shifted (Figure 1b). This observation can be attributed to the lattice expansion caused by the incorporation of Fe atoms into ZSM-5 framework with a larger bond length of Fe−O (1.86 Å) than a Al−O (1.73 Å) and Si−O bond (1.63 Å) ones.[17−19] SEM images show that, the [Fe,Al]ZSM-5 zeolites are characterized by an agglomeration of uniform nanocrystals (∼100 nm) up to 1.0 wt % Fe loading (Figure S2 top row). Further increase in Fe concertation in the initial gel and the addition of NaOH as a second mineralizing agent result in the formation of larger coffin-shaped crystals (∼0.5 μm) (Figure S2 bottom row) due to changes in kinetics of zeolite crystallization. According to TEM results, the presence of large Fe_2O_3 nanoparticles in fresh materials can be excluded (Figure S3).

UV−vis spectroscopy was applied to distinguish different Fe-species in the [Fe,Al]ZSM-5 samples. As demonstrated by Figure 2a, three types of Fe-species can be distinguished: (i)

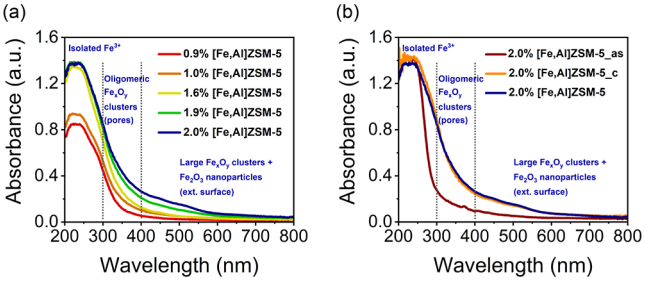

Figure 2. UV−vis spectra of (a) [Fe,Al]ZSM-5 catalysts with different Fe loadings and (b) three 2.0% [Fe,Al]ZSM-5 samples obtained under different conditions [as: as-synthesized sample, (c) sample obtained after calcination for template removal].

the high intensity/predominant absorbance peaks in the range of 200−300 nm, related to the isolated tetrahedrally/octahedrally coordinated Fe^{3+} sites in framework/extraframework positions;[20−22] (ii) weak features in the 300−400 nm region, attributed to the presence of oligomeric Fe_xO_y species within zeolite micropores;[23,24] and (iii) very weak features at > 400 nm, related to the presence of larger Fe_2O_3 clusters and nanoparticles.[23,25] The results further confirm that the majority of Fe-sites in [Fe,Al]ZSM-5 catalysts are isolated—either incorporated in the zeolite framework or at ion-exchange positions. Increasing the Fe loading leads to the formation of oligomeric Fe-oxide clusters and nanoparticles. These findings correlate well with the Ar physisorption results, where both the microporous areas and volumes of these catalysts slightly decrease with the increase in Fe loading (Table 1). In contrast, the UV−vis spectra of impregnated Fe/ZSM-5 catalysts exhibit broad bands between 200 and 600 nm (Figure S4), indicating the presence of Fe-species with various local structure and environments, including isolated Fe, oligomeric Fe_xO_y, and Fe_2O_3 nanoparticles.

To clarify the origin of the oligomeric Fe-species in [Fe,Al]ZSM-5 catalysts, we follow the three preparation steps of 2.0% [Fe,Al]ZSM-5 with UV−vis spectroscopy. Figure 2b shows UV−vis spectra for (i) an as-synthesized sample (2.0% [Fe,Al]ZSM-5_as); (ii) a sample obtained after the removal of organic template by calcination at 550 °C for 4 h (2.0% [Fe,Al]ZSM-5_c); and (iii) a sample obtained after further ion-exchange and another calcination at 550 °C for 7 h

https://doi.org/10.1021/acscatal.3c00854
ACS Catal. 2023, 13, 8128−8138

(2.0% [Fe,Al]ZSM-5). The results show that Fe_xO_y clusters and Fe_2O_3 nanoparticles are formed upon removal of the organic template, when some of Fe atoms are extracted from the ZSM-5 framework, while ion-exchange process and subsequent calcination do not lead to any significant changes.[26−28]

Next, we performed H_2-TPR experiments to understand the speciation of Fe in [Fe,Al]ZSM-5 samples (Figure 3). H_2-TPR

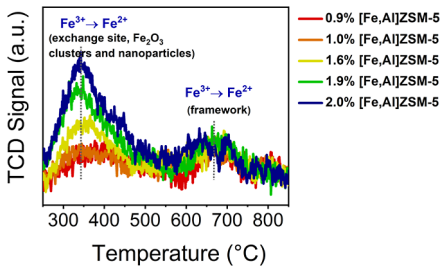

Figure 3. H_2-TPR profiles of [Fe,Al]ZSM-5 samples.

profiles of [Fe,Al]ZSM-5 catalysts show only two broad peaks, centered at 340 and 670 °C. According to the literature, the lower temperature peak corresponds to the reduction of Fe^{3+} at cationic exchange sites to Fe^{2+} and Fe_2O_3 clusters and nanoparticles to Fe^{2+}.[29−31] The latter agglomerated forms of Fe^{3+} are only present in low amounts in these samples. The high-temperature peak corresponds to the reduction of framework Fe^{3+} to Fe^{2+}.[32,33] This interpretation is supported by the H_2/Fe ratios being in the range of 0.4−0.5 (Table 2), which suggests that the majority of Fe^{3+} species in [Fe,Al]-ZSM-5 catalysts can only be partially reduced to a Fe^{2+} state in H_2.

Table 2. Metal Content, Brønsted Acidity, and H_2/Fe Ratios of [Fe,Al]ZSM-5 and Fe-Free ZSM-5

sample	Al[a] (μmol/g)	Fe[a] (μmol/g)	strong BAS[b] (μmol/g)	H_2/Fe[c] (mol/mol)
[Al]ZSM-5_N	281	–	150	–
[Al]ZSM-5	275	–	127	–
0.9% [Fe,Al]ZSM-5	266	156	406	0.4
1.0% [Fe,Al]ZSM-5	245	178	432	0.4
1.6% [Fe,Al]ZSM-5	282	278	323	0.4
1.9% [Fe,Al]ZSM-5	278	343	409	0.5
2.0% [Fe,Al]ZSM-5	253	348	408	0.5

[a]Al or Fe content determined by ICP analysis. [b]Strong BAS probed by Py-FTIR after a desorption step at 450 °C. [c]Molar ratio H_2/Fe consumption derived from TPR spectra.

The acidic properties of [Fe,Al]ZSM-5 catalysts were determined by FTIR spectroscopy of adsorbed pyridine, as shown in Tables 2 and S3. First, if compared to [Al]ZSM-5, the presence of Fe leads to a significant increase in the acidity of [Fe,Al]ZSM-5 catalysts (Table S3). Second, these catalysts also contain a large fraction of Brønsted acid sites (BAS, >80% of total acid sites) (Table S3). For example, the 0.9% [Fe,Al]ZSM-5 sample has an Al content of 266 μmol/g as determined by ICP, while the concentration of BAS measured by FTIR analysis of pyridine adsorption is 406 μmol/g (Table 2). This observation implies that the atomically dispersed Fe^{3+}-species in the zeolite framework contribute to the Brønsted acidity. In fact, the majority of Fe-atoms in [Fe,Al]ZSM-5 samples with Fe loading below 1.6 wt % are isomorphously substituted. Furthermore, as compared to [Al]ZSM-5, the number of BAS in impregnated Fe/ZSM-5 decreases (Table S3). This finding indicates that isolated Fe-species replace some of the protons at the exchange positions of ZSM-5.

To summarize, the above-mentioned data clearly show that [Fe,Al]ZSM-5 catalysts, prepared by direct hydrothermal synthesis, mainly contain two types of highly dispersed Fe-species, namely, (i) Fe^{3+} atoms incorporated in the zeolite framework and (ii) extraframework Fe^{3+} anchored at the exchange sites inside zeolite channels. The impregnated Fe/ZSM-5 sample contains a wider range of Fe-species, including extraframework Fe at exchange sites, oligomeric Fe_xO_y clusters, and Fe_2O_3 nanoparticles.

3.2. Catalytic Performance. Next, we investigated the MDA activity of the prepared catalysts at 700 °C. As shown by Figures 4a, S5, and S6, the activity and stability of [Fe,Al]ZSM-5 catalysts depend on the Fe loading. With the increase in Fe loading from 0.9 to 2.0 wt %, the induction period (time between the onset of benzene formation and the maximum benzene yield) was shortened from 500 to 100 min, accompanied by an increasing maximum benzene yield from 0.4 to 1.9% (Figure 4a). Among these [Fe,Al]ZSM-5 catalysts, 1.0% [Fe,Al]ZSM-5 shows the highest total amount of converted CH_4 (84.9 mmol/g) after 1000 min of the reaction (Table S4). [Fe,Al]ZSM-5 catalysts mainly convert methane into C_2 hydrocarbons (ethylene and ethane, >40%), benzene, toluene, and naphthalene (Figure 4b and Table S4). Although the benzene selectivity obtained over [Fe,Al]ZSM-5 catalyst remain moderate (≤30%), mainly due to the suboptimal high Si/Al ratio of ZSM-5 zeolite, the integral hydrocarbon selectivity is substantial (≥78%) with a coke selectivity of 13−22% (Table S4).

To facilitate the comparison of catalysts, the Fe/ZSM-5 and Mo/ZSM-5 samples prepared in this work contain the same molar concentration of transition metal atoms as in the corresponding [Fe,Al]ZSM-5 samples. Figures 4c,d and S7 show that the isomorphously substituted [Fe,Al]ZSM-5 catalysts exhibit a much higher integral hydrocarbon productivity compared to the impregnated Fe/ZSM-5 sample. Moreover, [Fe,Al]ZSM-5 show a better integral performance than Mo/ZSM-5 catalysts. For example, the 1.6% [Fe,Al]ZSM-5 catalyst exhibits a comparable maximum benzene yield of 1.9% to an impregnated Mo/ZSM-5 sample of the same molar metal loading (2.8% Mo/ZSM-5). Since [Fe,Al]ZSM-5 deactivates much slower than Mo/ZSM-5, it can convert a much larger amount of methane before complete deactivation. The rapid deactivation of the reference Mo/ZSM-5 catalysts explain their relatively low integral hydrocarbons productivity (Table S4). Regarding the improved catalytic performance of [Fe,Al]ZSM-5 and high abundance of Fe, catalytic systems based on Fe can be a promising alternative to the Mo-containing catalysts. In addition, Fe/ZSM-5 catalysts are much less prone to dealumination and structural degradation during oxidative regeneration as compared to Mo/ZSM-5.[34] We should note that the catalytic properties of Mo/ZSM-5 strongly depend on the Mo loading and Si/Al ratio of ZSM-5.[34,35] The MDA performance of Mo/ZSM-5 could be significantly improved by increasing the Mo loading and/or decreasing the bulk Si/Al ratio of the ZSM-5 zeolite.

https://doi.org/10.1021/acscatal.3c00854
ACS Catal. 2023, 13, 8128−8138

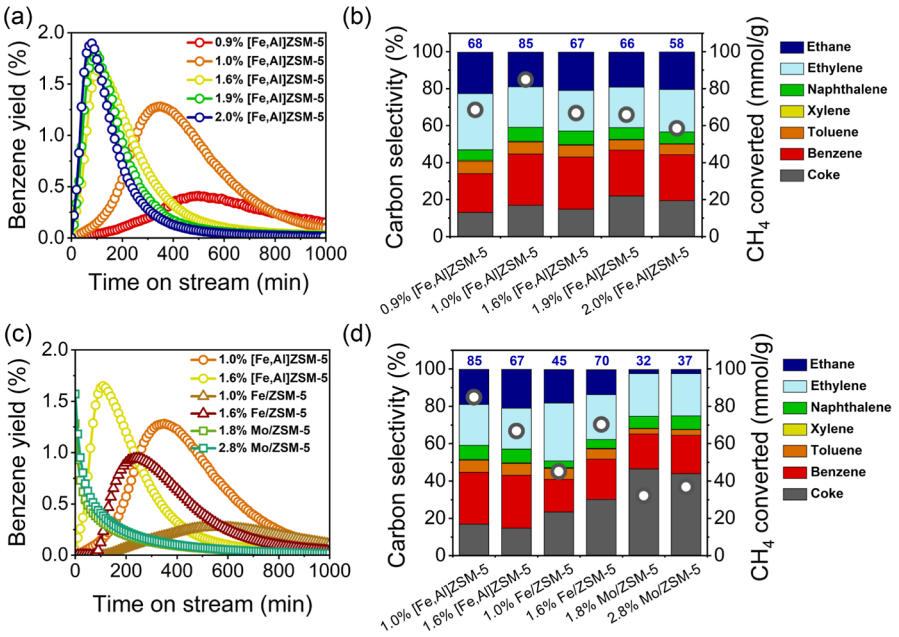

Figure 4. Benzene yield obtained during the MDA reaction for (a) [Fe,Al]ZSM-5 and (c) Fe/ZSM-5 and Mo/ZSM-5. Carbon selectivity to hydrocarbons and coke: (b) [Fe,Al]ZSM-5 and (d) Fe/ZSM-5 and Mo/ZSM-5. Conditions: 300 mg of catalyst, 700 °C, 30 mL/min of CH_4 flow, 1000 min, GC analysis.

Furthermore, the impregnated Fe/ZSM-5 samples show a much lower selectivity to hydrocarbons than the [Fe,Al]ZSM-5 ones (Figure 4d). Based on these findings, we can conclude that there exists a positive correlation between the MDA activity of Fe catalysts and the initial dispersion of Fe-species. The increased dispersion of Fe-sites in directly hydrothermally synthesized catalysts leads to a better MDA performance in comparison to the impregnated samples, likely because isolated Fe-species are precursors for highly active sites for the MDA reaction.

Recently, we have shown that the duration of the induction period in a series of Fe-, Mo-, and Re-modified zeolite catalysts can be linked to the generation of active hydrocarbon pool species.[16] In the hydrocarbon pool mechanism, methane is first activated on transition-metal sites to form hydrocarbon pool intermediates confined inside the zeolite pores and benzene is derived from the reaction of these species with the initial products (CH_x, C_2H_x, and H_2) of methane activation.[36,37] [Fe,Al]ZSM-5 displays a significantly shorter induction period as compared to Fe/ZSM-5, accompanied by a higher integral hydrocarbon productivity and a lower coke selectivity (Table S4). Considering that [Fe,Al]ZSM-5 contains more highly dispersed Fe-sites than Fe/ZSM-5, we speculate that a higher methane conversion rate leads to faster formation of the hydrocarbon pool precursors. In line with this, we also observe that increasing Fe loading in impregnated Fe/ZSM-5 samples results in a shorter induction period.

In summary, among the three types of catalysts studied here, [Fe,Al]ZSM-5 materials present the highest integral hydrocarbons productivity and methane conversion. The duration of the induction period is a reliable performance descriptor for the MDA activity of Fe-containing catalysts, in other words, Fe-containing ZSM-5 catalysts with a shorter induction period demonstrate higher catalytic activity.[16]

Stability tests were performed to determine the feasibility of reaction-regeneration cycling of the [Fe,Al]ZSM-5 catalysts. We used a reaction-regeneration protocol involving reaction in a CH_4 flow of 30 mL/min at 700 °C for 180 min and a regeneration process in diluted air (10 mL/min Air +20 mL/min He) for 60 min, either at 700 °C or 550 °C (Figure S8). Sufficient coke removal during regeneration was confirmed by TGA (<1 wt % coke remaining after regeneration at 550 °C, <0.01 wt % coke remaining after regeneration at 700 °C) and the absence of CO_2 in the reactor effluent as determined by GC (Figure S9). The reaction and regeneration steps were separated by He flushing (30 mL/min) for 30 min to avoid direct contact between CH_4 and air. A total of 10 reaction-regeneration cycles (50 h of operation in total) were conducted with 1.6% [Fe,Al]ZSM-5.

As shown by Figures 5a and S10, 1.6% [Fe,Al]ZSM-5 completely lost its activity after 15 h of MDA reaction. When the regeneration procedure is applied, both the CH_4 conversion and the yield of aromatics can be maintained at relatively high levels (Figure S10). After 10 cycles of reaction-regeneration, the decline of the initial activity is 49% when the regeneration is carried out at 700 °C and 37% at 550 °C (Figure 5b). Thus, oxidative regeneration at 550 °C is more favorable for preserving the catalytic activity of the 1.6% [Fe,Al]ZSM-5 catalyst. Figure S11 shows that the relative zeolite crystallinity of the used samples after 10 reaction-regeneration cycles remains high (> 96%), although additional peaks can be found at 2θ = 33.1, 35.6, and 40.8° to be attributed to the (1 0 4), (1 1 0), and (1 1 3) reflections of the hematite (Fe_2O_3, JCPDS: no. 033-0664) phase. UV−vis spectra of samples after reaction-regeneration confirm the deferration of the ZSM-5 framework and sintering of initially isolated Fe-species (Figure 5c). The micropore surface areas and volumes of these samples also slightly decrease, likely due to the pore blocking by the formed Fe_2O_3 particles (Table S5). Besides, a significant reduction in Brønsted acidity of 1.6% [Fe,Al]ZSM-5 after reaction-regeneration treatment is also observed at both regeneration temperatures (Figure 5d and Table S6), which can be related to the further removal of framework Fe^{3+} and the exchange of BAS with extraframework

https://doi.org/10.1021/acscatal.3c00854
ACS Catal. 2023, 13, 8128−8138

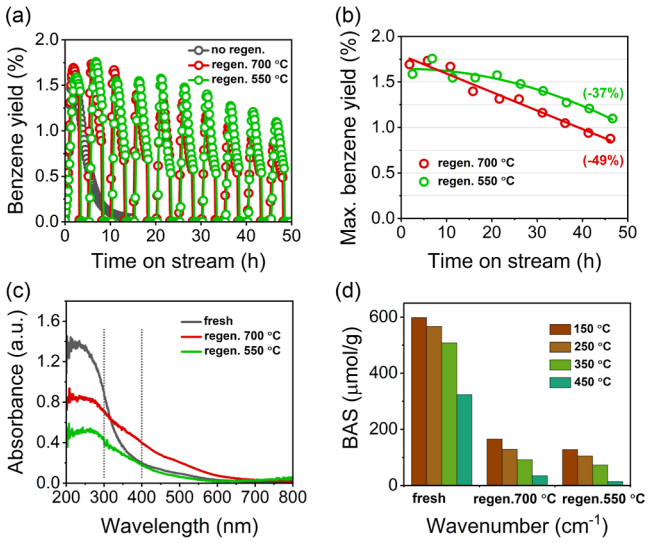

Figure 5. (a) Benzene yield obtained on 1.6% [Fe,Al]ZSM-5 catalyst during the reaction-regeneration cycles at different regeneration temperatures, (b) maximum benzene yields achieved in each reaction cycle, (c) UV−vis spectra, and (d) Brønsted acid sites determined by pyridine-FTIR for fresh and used 1.6% [Fe,Al]ZSM-5 samples after 10 reaction-regeneration cycles (50 h). Conditions: 300 mg of catalyst, 700 °C, GC analysis. For the regeneration conditions, see Figure S8.

Fe^{3+} ions. To summarize, the decrease of the MDA activity (−37 to −49% of the initial activity) during extended reaction-regeneration cycles can be attributed to the sintering of Fe-species. Regeneration strategies involving milder coke combustion or intermittent re-dispersion of Fe-species can be potentially used to improve the reaction-regeneration stability of [Fe,Al]ZSM-5.[38−40]

3.3. Active Fe-Sites in [Fe,Al]ZSM-5. To further understand the catalytic performance of [Fe,Al]ZSM-5 catalysts and their limited reaction-regeneration stability, it is necessary to identify the active Fe-species. We studied the evolution of the Fe-sites during the reaction and regeneration by operando XANES spectroscopy coupled with MS. Figure 6a shows XANES spectra recorded during exposing the 1.0% [Fe,Al]ZSM-5 catalyst to CH_4 flow of 5 mL/min, heating the catalyst to 700 °C and maintaining the sample at 700 °C for the MDA reaction.

The spectra display a gradual shift of the rising edge feature to a lower energy with the increase in temperature and exposure time (Figure 6a). This shift corresponds to the reduction of Fe-atoms.[41] By comparing the edge positions of these spectra with that for iron oxides (Figure S12), we conclude that Fe is reduced from the initial Fe^{3+} state to a Fe^{2+} state during the reaction.[42] The pre-edge region of XANES spectra (inset of Figure 6a), corresponding to 1s → 3d electronic transitions, is particularly useful for analyzing the oxidation state and geometry of Fe-species.[43] High-energy-resolution fluorescence detection (HERFD)-XANES is considered the most suitable method to study the pre-edges of Fe-compounds and Fe/ZSM-5, in particular.[44,45] Recently, Boubnov et al. compared the utility of HERFD-XANES and conventional transmission XANES for the analysis of the pre-edge regions of various Fe compounds.[46] The authors analyzed the pre-edge spectra of various reference materials and used the pre-edge centroid energy and the integrated pre-edge intensity to describe the oxidation state and geometry of Fe-sites. The centroid position describes the oxidation state, which is either Fe^{2+} (energy range 7112.6−7113.3 eV) or Fe^{3+} (7114.0−7114.5 eV). In turn, the integrated pre-edge intensity corresponds to either tetrahedral (integrated pre-edge intensity values from 0.2 to 0.36) or octahedral (0.04−0.15) coordination of Fe^{2+} or Fe^{3+} atoms. The authors confirmed that transmission XANES can also be used for the accurate determination of oxidation and coordination of Fe-atoms. Our analysis of several reference compounds is in line with these findings (Figure S13).

We analyzed the pre-edge regions of XANES spectra obtained during the operando experiments (see Figure S14 for fitting models) to track the changes in the oxidation state and geometry of Fe-species during the MDA reaction. Figure 6b shows the pre-edge centroid values and integrated intensity together with the MS signals of H_2 (m/z = 2) and benzene (m/z = 78) simultaneously recorded during the operando XANES-MS experiment on 1.0% [Fe,Al]ZSM-5. Initially, tetrahedral Fe^{3+} species are present in the framework/extraframework positions of 1.0% [Fe,Al]ZSM-5 sample and the structure of these species does not significantly change until the temperature reaches 500 °C (Figure 6b). After that, a gradual decrease in both pre-edge centroid and integrated intensity values takes place. This decrease can be assigned to the slow formation of octahedral Fe^{2+} species. Compared to the evolution of the MS signal of H_2, which is proportional to the rate of non-oxidative methane conversion, and coincides with the transformation of Fe-species, the benzene formation is delayed (inset of Figure 6b). We note that the sharp peak of

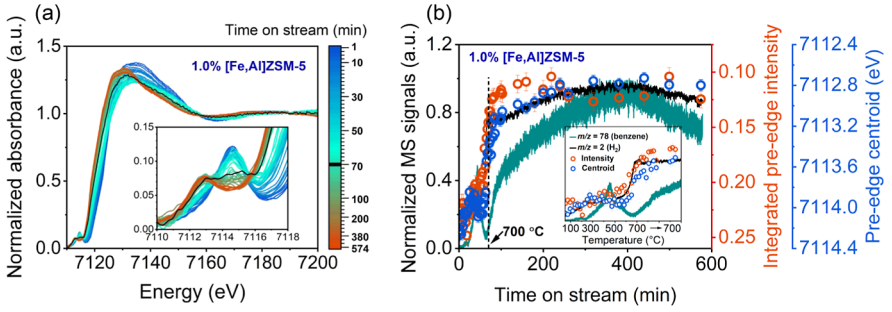

Figure 6. (a) Operando Fe K-edge XANES spectra recorded over 1.0% [Fe,Al]ZSM-5 catalyst during the MDA reaction and (b) comparison of pre-edge integrated intensity and centroid values with simultaneously recorded MS signals of H_2 (m/z = 2) and benzene (m/z = 78). Conditions: 10 mg of 1.0% [Fe,Al]ZSM-5, 700 °C (ramp rate 10 °C/min, total ramping time of ∼70 min), 5 mL/min of CH_4 flow. Black spectrum (a) and dash line (b) correspond to the time when 700 °C was reached.

https://doi.org/10.1021/acscatal.3c00854
ACS Catal. 2023, 13, 8128−8138

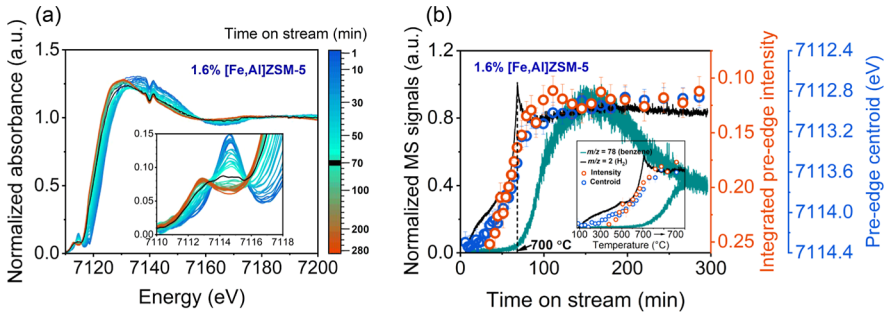

Figure 7. (a) Operando Fe K-edge XANES spectra collected over 1.6% [Fe,Al]ZSM-5 catalyst during the MDA reaction and (b) comparison of pre-edge integrated intensity and centroid values with simultaneously recorded MS signals of H_2 (m/z = 2) and benzene (m/z = 78). Conditions: 10 mg 1.6% [Fe,Al]ZSM-5, 700 °C (ramp rate 10 °C/min, total ramping time of ~70 min), 5 mL/min of CH_4 flow. Prior to the MDA reaction, the 1.6% [Fe,Al]ZSM-5 catalyst was pre-treated in air at 550 °C for 30 min. Black spectrum (a) and dash line (b) correspond to the time when 700 °C was reached.

benzene production between 300 and 700 °C corresponds to the aromatization and desorption of hydrocarbon molecules initially adsorbed in the zeolite pores and is not related to the catalytic methane dehydroaromatization. As the formation of benzene only starts at 700 °C, we can infer that the onset of benzene formation does not correlate with the reduction of Fe-sites. The increase in benzene concentration (i.e., induction period) continues for another ~300 min, in line with the catalytic results (Figure 4a). After the initial reduction, Fe-species remain in the same octahedral Fe^{2+} state during the induction period and the subsequent deactivation stage of the reaction (Figure 6b). Similar behavior was observed for the 1.6% [Fe,Al]ZSM-5 catalyst with a higher Fe loading (Figure 7). We note that this catalyst was calcined in O_2 at 550 °C prior to the operando XANES experiment, so the sharp peak of benzene in MS is absent. Altogether, these results demonstrate that the actual active Fe-species in the working [Fe,Al]ZSM-5 catalyst comprise Fe^{2+} species in octahedral coordination. Based on these observations and congruent with literature reports, a reasonable hypothesis is Fe (2+)-carbides or Fe (2+)-oxy-carbides.[8,10,13]

By comparing the catalytic behavior of 1.0% [Fe,Al]ZSM-5 with 1.0% Fe/ZSM-5 (Figure S15 for operando XANES-MS data), we observe that Fe^{3+} atoms in the latter catalyst are initially present in octahedral coordination (integrated pre-edge intensity of ~0.15). In line with the UV−vis (Figure 5c) and EXAFS (Figure S16) results, this state mainly corresponds to Fe_2O_3 clusters and nanoparticles.[45] These agglomerated forms of Fe are more reducible than isomporphously substituted Fe-atoms (Figure 8) and lead to the formation of less active Fe-species as manifested by the lower benzene yields obtained over impregnated samples (Figure 4c). Interestingly, upon regeneration of used [Fe,Al]ZSM-5 catalysts in O_2 (Figures S17 and S18), another type of tetrahedral Fe^{3+} species is formed according to EXAFS data (Figure S19). These species are much more reducible than the initially isomorphously substituted Fe-atoms (Figures 8 and S20) and gradually lose their catalytic activity during subsequent reaction-regeneration cycles (Figure 5a). Based on the appearance of bands in UV−vis spectra (Figure 5c), a decrease of the overall Brønsted acidity (Figure 5d and Table S6), and the changes in EXAFS spectra (Figure S19), we can reasonably conclude that isomorphously substituted Fe-atoms leave the framework positions and form small Fe_2O_3 clusters during oxidative regeneration. Although catalysts gradually lose their activity, the small Fe_2O_3 clusters are still far more active than

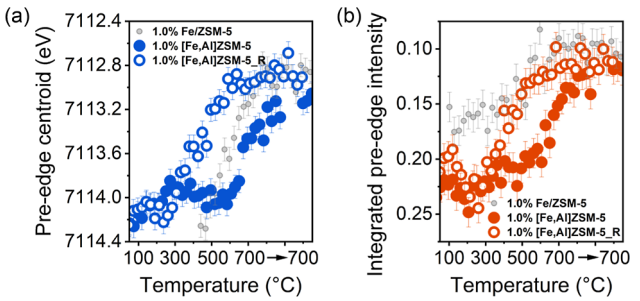

Figure 8. Pre-edge centroid (a) and intensity (b) values obtained during the MDA reaction over 1.0% [Fe,Al]ZSM-5 (1.0% [Fe,Al]-ZSM-5), 1.0% [Fe,Al]ZSM-5 after the MDA reaction for 8 h and regeneration in air at 550 °C (1.0% [Fe,Al]ZSM-5_R), and 1.0% Fe/ZSM-5 sample (1.0% Fe/ZSM-5). Conditions: 10 mg of catalyst, 700 °C (ramp rate 10 °C/min), 5 mL/min of CH_4 flow.

Fe -clusters on their counterparts prepared by impregnation, even after 10 reaction-regeneration cycles (Figure 5a).

Overall, it can be concluded that the initial tetrahedral Fe^{3+} within the zeolite framework or at exchange sites are transformed to extraframework octahedral Fe^{2+}, which are the active Fe-sites for methane aromatization. The isomorphously substituted Fe can also leave the framework positions to form small Fe_2O_3 clusters during oxidative regeneration.

3.4. Evolution of Surface Carbon on [Fe,Al]ZSM-5 Catalysts. Since the extensive coke formation is responsible for the deactivation of [Fe,Al]ZSM-5 catalysts, we followed the growth of carbon deposits and their properties using operando TGA-MS and ex situ TGA. As demonstrated by Figure 9, for all [Fe,Al]ZSM-5 catalysts, a two-step weight increase can be observed in the TG/DTG curves: (i) a rapid weight gain stage, due to the fast generation of hydrocarbon pool species inside ZSM-5 pores and (ii) a slow weight increase stage, corresponding to the formation of deactivating coke species.[47] In line with the catalytic results (Figure 4a), we observed that the length of the rapid weight gain stage is reduced from 186 to 111 min, by increasing the Fe content from 0.9 to 1.6 wt %. We should note that the duration of this period for impregnated Fe/ZSM-5 catalysts can be as high as 1000 min under the same reaction conditions.[16] Therefore, we can conclude that the improved Fe dispersion leads to a faster formation of active hydrocarbon pool intermediates, significantly shortening the induction period. This observation correlates well with the catalytic performance of catalysts shown in Figure 4c. In terms of MS signal, the production of

https://doi.org/10.1021/acscatal.3c00854
ACS Catal. 2023, 13, 8128−8138

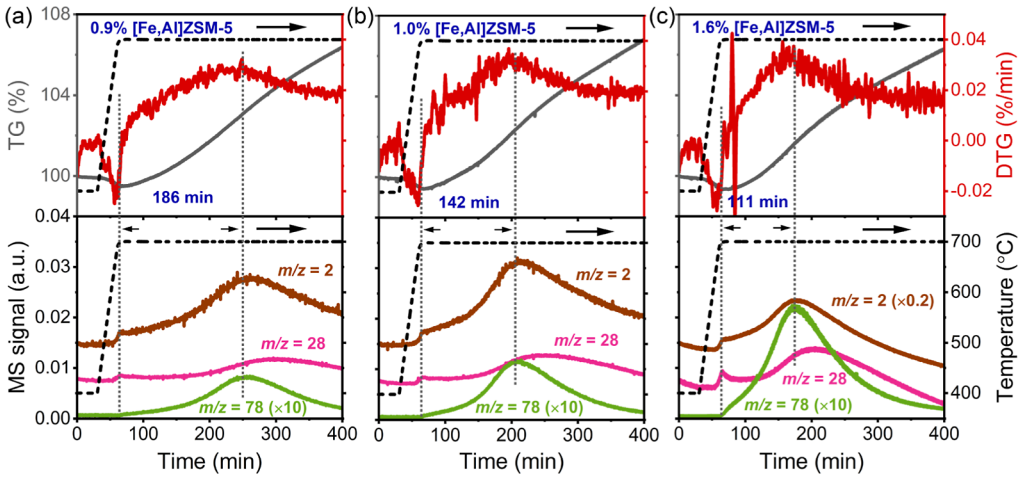

Figure 9. TG/DTG profiles and corresponding MS signals recorded during the operando TGA-MS experiment: (a) 0.9% [Fe,Al]ZSM-5, (b) 1.0% [Fe,Al]ZSM-5, and (c) 1.6% [Fe,Al]ZSM-5.

H_2 (m/z = 2) and benzene (m/z = 78) reaches a maximum (induction period), followed by a gradual decrease due to catalyst deactivation. The duration of the induction period is in line with the fast weight gain stage for all [Fe,Al]ZSM-5 catalysts. This duration also reduces with the increase in Fe dispersion and loading, accompanied by enhanced benzene production, due to the faster growth of hydrocarbon pool components.

TG profiles of the spent [Fe,Al]ZSM-5 catalysts after complete deactivation were also recorded. Figure 10a shows

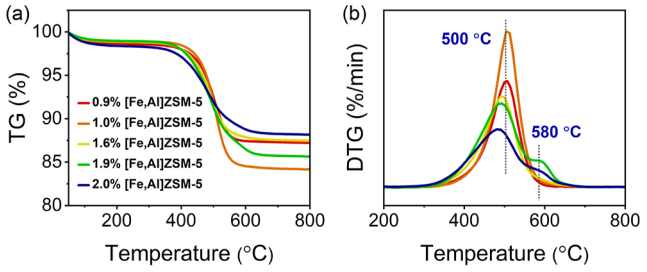

Figure 10. TG (a) and DTG (b) profiles of spent [Fe,Al]ZSM-5 catalysts.

that the total amount of coke does not strongly correlate with the Fe loading and that the catalysts can accumulate 10−15 wt % of coke. The main combustion peaks in DTG profiles of [Fe,Al]ZSM-5 catalysts are around 500 °C (Figure 10b). For samples with an Fe loading > 1.6 wt %, an additional combustion peak centered at 590 °C appeared. This peak is most likely related to the carbon nanofibers formed on the zeolite external surface, which require a higher combustion temperature.[48] As these carbon nanofibers are especially abundant on impregnated Fe samples (Figure S21), we can correlate their formation with the larger Fe clusters present on the external surface of [Fe,Al]ZSM-5 catalysts with higher Fe loading.

4. CONCLUSIONS

[Fe,Al]ZSM-5 were prepared by direct hydrothermal synthesis and compared to Fe/ZSM-5 and Mo/ZSM-5 samples prepared by impregnation. Fe^{3+} species in [Fe,Al]ZSM-5 are either isomorphously substituted in the ZSM-5 framework contributing to Brønsted acidity, or anchored at cationic exchange sites inside the zeolite pores. Impregnated Fe/ZSM-5 catalysts consist of a wider range of Fe-species including extraframework Fe at exchange sites, oligomeric Fe_xO_y clusters and Fe_2O_3 nanoparticles. [Fe,Al]ZSM-5 catalysts show a higher integral hydrocarbons productivity than the Mo/ZSM-5 and Fe/ZSM-5 references at the same molar metal loading. The increasing dispersion and loading of Fe-species results in a shorter induction period and an overall better MDA performance. Reaction-regeneration experiments show that oxidative regeneration at 550 °C is an effective way to remove coke, while maintaining high MDA activity of [Fe,Al]ZSM-5 catalysts. The slowly decreasing MDA activity during reaction-regeneration cycles is due to the deferration of the zeolite framework and sintering of the initially isolated Fe-species. Operando XANES-MS and EXAFS show that isolated Fe^{3+} species in the [Fe,Al]ZSM-5 framework or at exchange sites in tetrahedral coordination are converted into extraframework active Fe^{2+} species in octahedral coordination during the MDA reaction and form small Fe_2O_3 clusters during oxidative regeneration. The duration of the induction period correlates well with the MDA activity of [Fe,Al]ZSM-5 catalysts, while Fe dispersion and loading are the most important activity descriptors. The present findings provide useful insights for designing Fe/ZSM-5 catalysts with enhanced catalytic properties.

■ ASSOCIATED CONTENT

Supporting Information

The Supporting Information is available free of charge at https://pubs.acs.org/doi/10.1021/acscatal.3c00854.

ICP results, carbon selectivity, SEM/TEM images, UV−vis spectra, Py-FTIR results, catalytic test, Ar physisorption data, XRD patterns, operando XANES-MS, EXAFS analysis, and TG/DTG profiles (PDF)

■ AUTHOR INFORMATION

Corresponding Author

Nikolay Kosinov − *Laboratory of Inorganic Materials & Catalysis, Department of Chemical Engineering and Chemistry, Eindhoven University of Technology, Eindhoven 5600 MB, The Netherlands;* orcid.org/0000-0001-8520-4886; Phone: +31-40-2478156; Email: n.a.kosinov@tue.nl

https://doi.org/10.1021/acscatal.3c00854
ACS Catal. 2023, 13, 8128−8138

Authors

Yujie Liu − *Laboratory of Inorganic Materials & Catalysis, Department of Chemical Engineering and Chemistry, Eindhoven University of Technology, Eindhoven 5600 MB, The Netherlands*

Aleksei Bolshakov − *Laboratory of Inorganic Materials & Catalysis, Department of Chemical Engineering and Chemistry, Eindhoven University of Technology, Eindhoven 5600 MB, The Netherlands;* orcid.org/0000-0001-7483-2916

Marita Ćoza − *Laboratory of Inorganic Materials & Catalysis, Department of Chemical Engineering and Chemistry, Eindhoven University of Technology, Eindhoven 5600 MB, The Netherlands;* orcid.org/0009-0008-6090-8172

Victor Drozhzhin − *Laboratory of Inorganic Materials & Catalysis, Department of Chemical Engineering and Chemistry, Eindhoven University of Technology, Eindhoven 5600 MB, The Netherlands*

Emiel J. M. Hensen − *Laboratory of Inorganic Materials & Catalysis, Department of Chemical Engineering and Chemistry, Eindhoven University of Technology, Eindhoven 5600 MB, The Netherlands;* orcid.org/0000-0002-9754-2417

Complete contact information is available at: https://pubs.acs.org/10.1021/acscatal.3c00854

Notes

The authors declare no competing financial interest.

■ ACKNOWLEDGMENTS

We would like to thank China Scholarship Council (no. 201806930028) for the financial support. We also acknowledge the MAX IV Laboratory for provision of synchrotron radiation facilities and Dr. Konstantin Klementiev for his assistance with the measurements. We also thank Dr. Valery Muravev and Yu Gao for their help with synchrotron experiments.

■ REFERENCES

(1) Olivos-Suarez, A. I.; Szécsényi, À.; Hensen, E. J. M.; Ruiz-Martinez, J.; Pidko, E. A.; Gascon, J. Strategies for the Direct Catalytic Valorization of Methane Using Heterogeneous Catalysis: Challenges and Opportunities. *ACS Catal.* **2016**, *6*, 2965−2981.

(2) Ismagilov, Z. R.; Matus, E. V.; Tsikoza, L. T. Direct Conversion of Methane on Mo/ZSM-5 Catalysts to Produce Benzene and Hydrogen: Achievements and Perspectives. *Energy Environ. Sci.* **2008**, *1*, 526−541.

(3) Spivey, J. J.; Hutchings, G. Catalytic Aromatization of Methane. *Chem. Soc. Rev.* **2014**, *43*, 792−803.

(4) Kosinov, N.; Hensen, E. J. M. Reactivity, Selectivity, and Stability of Zeolite-Based Catalysts for Methane Dehydroaromatization. *Adv. Mater.* **2020**, *32*, 2002565.

(5) Weckhuysen, B. M.; Wang, D.; Rosynek, M. P.; Lunsford, J. H. Conversion of Methane to Benzene over Transition Metal Ion ZSM-5 Zeolites: I. Catalytic Characterization. *J. Catal.* **1998**, *175*, 338−346.

(6) Denardin, F.; Perez-Lopez, O. W. Tuning the Acidity and Reducibility of Fe/ZSM-5 Catalysts for Methane Dehydroaromatization. *Fuel* **2019**, *236*, 1293−1300.

(7) Weckhuysen, B. M.; Wang, D.; Rosynek, M. P.; Lunsford, J. H. Catalytic Conversion of Methane into Aromatic Hydrocarbons over Iron Oxide Loaded ZSM-5 Zeolites. *Angew. Chem., Int. Ed. Engl.* **1997**, *36*, 2374−2376.

(8) Tan, P. Active Phase, Catalytic Activity, and Induction Period of Fe/Zeolite Material in Nonoxidative Aromatization of Methane. *J. Catal.* **2016**, *338*, 21−29.

(9) Guo, X.; Fang, G.; Li, G.; Ma, H.; Fan, H.; Yu, L.; Ma, C.; Wu, X.; Deng, D.; Wei, M.; Tan, D.; Si, R.; Zhang, S.; Li, J.; Sun, L.; Tang, Z.; Pan, X.; Bao, X. Direct, Nonoxidative Conversion of Methane to Ethylene, Aromatics, and Hydrogen. *Science* **2014**, *344*, 616−619.

(10) Vollmer, I.; Ould-Chikh, S.; Aguilar-Tapia, A.; Li, G.; Pidko, E.; Hazemann, J. L.; Kapteijn, F.; Gascon, J. Activity Descriptors Derived from Comparison of Mo and Fe as Active Metal for Methane Conversion to Aromatics. *J. Am. Chem. Soc.* **2019**, *141*, 18814−18824.

(11) Xu, Y.; Yuan, X.; Chen, M.; Dong, A.; Liu, B.; Jiang, F.; Yang, S.; Liu, X. Identification of Atomically Dispersed Fe-Oxo Species as New Active Sites in HZSM-5 for Efficient Non-Oxidative Methane Dehydroaromatization. *J. Catal.* **2021**, *396*, 224−241.

(12) Lai, Y.; Veser, G. The Nature of the Selective Species in Fe-HZSM-5 for Non-Oxidative Methane Dehydroaromatization. *Catal. Sci. Technol.* **2016**, *6*, 5440−5452.

(13) Gu, Y.; Chen, P.; Wang, X.; Lyu, Y.; Liu, W.; Liu, X.; Yan, Z. Active Sites and Induction Period of Fe/ZSM-5 Catalyst in Methane Dehydroaromatization. *ACS Catal.* **2021**, *11*, 6771−6786.

(14) Kiani, D.; Sourav, S.; Tang, Y.; Baltrusaitis, J.; Wachs, I. E. Methane Activation by ZSM-5-Supported Transition Metal Centers. *Chem. Soc. Rev.* **2021**, *50*, 1251−1268.

(15) Ravel, B.; Newville, M. ATHENA, ARTEMIS, HEPHAESTUS: Data Analysis for X-Ray Absorption Spectroscopy Using IFEFFIT. *J. Synchrotron Radiat.* **2005**, *12*, 537−541.

(16) Liu, Y.; Ćoza, M.; Drozhzhin, V.; Van Den Bosch, Y.; Meng, L.; Van De Poll, R.; Hensen, E. J. M.; Kosinov, N. Transition-Metal Catalysts for Methane Dehydroaromatization (Mo, Re, Fe): Activity, Stability, Active Sites, and Carbon Deposits. *ACS Catal.* **2022**, *13*, 1−10.

(17) Taboada, J. B.; Overweg, A. R.; Crajé, M. W. J.; Arends, I. W. C. E.; Mul, G.; Van Der Kraan, A. M. Systematic Variation Of57Fe and Al Content in Isomorphously Substituted57FeZSM-5 Zeolites: Preparation and Characterization. *Microporous Mesoporous Mater.* **2004**, *75*, 237−246.

(18) Jiang, X.; Su, X.; Bai, X.; Li, Y.; Yang, L.; Zhang, K.; Zhang, Y.; Liu, Y.; Wu, W. Conversion of Methanol to Light Olefins over Nanosized [Fe,Al]ZSM-5 Zeolites: Influence of Fe Incorporated into the Framework on the Acidity and Catalytic Performance. *Microporous Mesoporous Mater.* **2018**, *263*, 243−250.

(19) Berlier, G.; Spoto, G.; Bordiga, S.; Ricchiardi, G.; Fisicaro, P.; Zecchina, A.; Rossetti, I.; Selli, E.; Forni, L.; Giamello, E.; Lamberti, C. Evolution of Extraframework Iron Species in Fe Silicalite: 1. Effect of Fe Content, Activation Temperature, and Interaction with Redox Agents. *J. Catal.* **2002**, *208*, 64−82.

(20) Yu, T.; Li, Z.; Jones, W.; Liu, Y.; He, Q.; Song, W.; Du, P.; Yang, B.; An, H.; Farmer, D. M.; Qiu, C.; Wang, A.; Weckhuysen, B. M.; Beale, A. M.; Luo, W. Identifying Key Mononuclear Fe Species for Low-Temperature Methane Oxidation. *Chem. Sci.* **2021**, *12*, 3152−3160.

(21) Iwasaki, M.; Yamazaki, K.; Banno, K.; Shinjoh, H. Characterization of Fe/ZSM-5 $DeNO_x$ Catalysts Prepared by Different Methods: Relationships between Active Fe Sites and NH_3-SCR Performance. *J. Catal.* **2008**, *260*, 205−216.

(22) Sun, K.; Xia, H.; Feng, Z.; van Santen, R.; Hensen, E.; Li, C. Active Sites in Fe/ZSM-5 for Nitrous Oxide Decomposition and Benzene Hydroxylation with Nitrous Oxide. *J. Catal.* **2008**, *254*, 383−396.

(23) Hammond, C.; Dimitratos, N.; Jenkins, R. L.; Lopez-Sanchez, J. A.; Kondrat, S. A.; Hasbi Ab Rahim, M.; Forde, M. M.; Thetford, A.; Taylor, S. H.; Hagen, H.; Stangland, E. E.; Kang, J. H.; Moulijn, J. M.; Willock, D. J.; Hutchings, G. J. Elucidation and Evolution of the Active Component within Cu/Fe/ZSM-5 for Catalytic Methane Oxidation: From Synthesis to Catalysis. *ACS Catal.* **2013**, *3*, 689−699.

(24) Lim, J. B.; Cha, S. H.; Hong, S. B. Direct N_2O Decomposition over Iron-Substituted Small-Pore Zeolites with Different Pore Topologies. *Appl. Catal. B Environ.* **2019**, *243*, 750−759.

(25) Meng, L.; Zhu, X.; Hensen, E. J. M. Stable Fe/ZSM-5 Nanosheet Zeolite Catalysts for the Oxidation of Benzene to Phenol. *ACS Catal.* **2017**, *7*, 2709−2719.
(26) Berlier, G.; Zecchina, A.; Spoto, G.; Ricchiardi, G.; Bordiga, S.; Lamberti, C. The Role of Al in the Structure and Reactivity of Iron Centers in Fe-ZSM-5-Based Catalysts: A Statistically Based Infrared Study. *J. Catal.* **2003**, *215*, 264−270.
(27) Mul, G.; Pérez-Ramírez, J.; Kapteijn, F.; Moulijn, J. A. NO Adsorption on Ex-Framework [Fe, X]MFI Catalysts: Novel IR Bands and Evaluation of Assignments. *Catal. Lett.* **2002**, *80*, 129−138.
(28) Hensen, E. J. M.; Zhu, Q.; Janssen, R. A. J.; Magusin, P. C. M. M.; Kooyman, P. J.; Van Santen, R. A. Selective Oxidation of Benzene to Phenol with Nitrous Oxide over MFI Zeolites: 1. on the Role of Iron and Aluminum. *J. Catal.* **2005**, *233*, 123−135.
(29) Delahay, G.; Valade, D.; Guzmán-Vargas, A.; Coq, B. Selective Catalytic Reduction of Nitric Oxide with Ammonia on Fe-ZSM-5 Catalysts Prepared by Different Methods. *Appl. Catal. B Environ.* **2005**, *55*, 149−155.
(30) Li, Y.; Feng, Z.; Xin, H.; Fan, F.; Zhang, J.; Magusin, P. C. M. M.; Hensen, E. J. M.; Van Santen, R. A.; Yang, Q.; Li, C. Effect of Aluminum on the Nature of the Iron Species in Fe-SBA-15. *J. Phys. Chem. B* **2006**, *110*, 26114−26121.
(31) Krishna, K.; Seijger, G. B. F.; Van den Bleek, C. M.; Makkee, M.; Mul, G.; Calis, H. P. A. Selective Catalytic Reduction of NO with NH_3 over Fe-ZSM-5 Catalysts Prepared by Sublimation of $FeCl_3$ at Different Temperatures. *Catal. Lett.* **2003**, *86*, 121−132.
(32) Pérez-Ramírez, J.; Mul, G.; Kapteijn, F.; Moulijn, J. A.; Overweg, A. R.; Doménech, A.; Ribera, A.; Arends, I. W. C. E. Physicochemical Characterization of Isomorphously Substituted FeZSM-5 during Activation. *J. Catal.* **2002**, *207*, 113−126.
(33) Bordiga, S.; Buzzoni, R.; Geobaldo, F.; Lamberti, C.; Giamello, E.; Zecchina, A.; Leofanti, G.; Petrini, G.; Tozzola, G.; Vlaic, G. Structure and Reactivity of Framework and Extraframework Iron in Fe-Silicalite as Investigated by Spectroscopic and Physicochemical Methods. *J. Catal.* **1996**, *158*, 486−501.
(34) Kosinov, N.; Coumans, F. J. A. G.; Li, G.; Uslamin, E.; Mezari, B.; Wijpkema, A. S. G.; Pidko, E. A.; Hensen, E. J. M. Stable Mo/HZSM-5 Methane Dehydroaromatization Catalysts Optimized for High-Temperature Calcination-Regeneration. *J. Catal.* **2017**, *346*, 125−133.
(35) Liu, S.; Wang, L.; Ohnishi, R.; Ichikawa, M. Bifunctional Catalysis of Mo/HZSM-5 in the Dehydroaromatization of Methane to Benzene and Naphthalene XAFS/TG/DTA/MASS/FTIR Characterization and Supporting Effects. *J. Catal.* **1999**, *181*, 175−188.
(36) Kosinov, N.; Wijpkema, A. S. G.; Uslamin, E.; Rohling, R.; Coumans, F. J. A. G.; Mezari, B.; Parastaev, A.; Poryvaev, A. S.; Fedin, M. V.; Pidko, E. A.; Hensen, E. J. M. Confined Carbon Mediating Dehydroaromatization of Methane over Mo/ZSM-5. *Angew. Chem., Int. Ed.* **2018**, *57*, 1016−1020.
(37) Vollmer, I.; Li, G.; Yarulina, I.; Kosinov, N.; Hensen, E. J.; Houben, K.; Mance, D.; Baldus, M.; Gascon, J.; Kapteijn, F. Relevance of the Mo-Precursor State in H-ZSM-5 for Methane Dehydroaromatization. *Catal. Sci. Technol.* **2018**, *8*, 916−922.
(38) Zhang, Y.; Jiang, H. A Novel Route to Improve Methane Aromatization by Using a Simple Composite Catalyst. *Chem. Commun.* **2018**, *54*, 10343−10346.
(39) Portilla, M. T.; Llopis, F. J.; Martínez, C. Non-Oxidative Dehydroaromatization of Methane: An Effective Reaction-Regeneration Cyclic Operation for Catalyst Life Extension. *Catal. Sci. Technol.* **2015**, *5*, 3806−3821.
(40) Kosinov, N.; Coumans, F. J. A. G.; Uslamin, E.; Kapteijn, F.; Hensen, E. J. M. Selective Coke Combustion by Oxygen Pulsing During Mo/ZSM-5-Catalyzed Methane Dehydroaromatization. *Angew. Chem., Int. Ed.* **2016**, *55*, 15086−15090.
(41) Sarangi, R. X-ray Absorption near-Edge Spectroscopy in Bioinorganic Chemistry: Application to M-O_2 Systems. *Coord. Chem. Rev.* **2013**, *257*, 459−472.
(42) Hensen, E.; Zhu, Q.; Liu, P. H.; Chao, K. J.; Van Santen, R. On the Role of Aluminum in the Selective Oxidation of Benzene to Phenol by Nitrous Oxide over Iron-Containing MFI Zeolites: An in Situ Fe XANES Study. *J. Catal.* **2004**, *226*, 466−470.
(43) Westre, T. E.; Kennepohl, P.; DeWitt, J. G.; Hedman, B.; Hodgson, K. O.; Solomon, E. I. A Multiplet Analysis of Fe K-Edge 1s → 3d Pre-Edge Features of Iron Complexes. *J. Am. Chem. Soc.* **1997**, *119*, 6297−6314.
(44) Heijboer, W. M.; Koningsberger, D. C.; Weckhuysen, B. M.; Groot, F. d. New Frontiers in X-Ray Spectroscopy in Heterogeneous Catalysis: Using Fe/ZSM-5 as Test-System. *Catal. Today* **2005**, *110*, 228−238.
(45) Boubnov, A.; Carvalho, H. W. P.; Doronkin, D. E.; Gu, T.; Gallo, E.; Atkins, A. J.; Jacob, C. R.; Grunwaldt, J. Selective Catalytic Reduction of NO Over Fe-ZSM-5 : Mechanistic. *J. Am. Chem. Soc.* **2014**, *136*, 13006−13015.
(46) Boubnov, A.; Lichtenberg, H.; Mangold, S.; Grunwaldt, J. D. Identification of the Iron Oxidation State and Coordination Geometry in Iron Oxide- and Zeolite-Based Catalysts Using Pre-Edge XAS Analysis. *J. Synchrotron Radiat.* **2015**, *22*, 410−426.
(47) Liu, Y.; Zhang, H.; Wijpkema, A. S. G.; Coumans, F. J. A. G.; Meng, L.; Uslamin, E. A.; Longo, A.; Hensen, E. J. M.; Kosinov, N. Understanding the Preparation and Reactivity of Mo/ZSM-5 Methane Dehydroaromatization Catalysts. *Chem.—A Eur. J.* **2022**, *28*, No. e202103894.
(48) Sridhar, A.; Rahman, M.; Khatib, S. J. Enhancement of Molybdenum/ZSM-5 Catalysts in Methane Aromatization by the Addition of Iron Promoters and by Reduction/Carburization Pretreatment. *ChemCatChem* **2018**, *10*, 2571−2583.

https://doi.org/10.1021/acscatal.3c00854
ACS Catal. 2023, 13, 8128−8138